International Journal of Nanomedicine

Dovepress
Taylor & Francis Group

Open Access Full Text Article

ORIGINAL RESEARCH

An Injectable Hydrogel Bioimplant Loaded with Engineered Exosomes and Triple Anti-Tuberculosis Drugs with Potential for Treating Bone and Joint Tuberculosis

Jiayan Huang[1,*], Han Li[2,*], Yuting Mei[1], Pengcheng Yi[1], Yunyao Ren[1], Yunjuan Wang[3], Limei Han[1], Qiusha Tang[3], Dongfang Liu[3], Wei Chen[4], Yanli An[5], Chunmei Hu[1]

[1]Department of Tuberculosis, the Second Hospital of Nanjing, Affiliated to Nanjing University of Chinese Medicine, Nanjing, People's Republic of China; [2]Department of Pharmacy, Central Hospital of Guangdong Provincial Nongken, Zhanjiang, Guangdong, People's Republic of China; [3]Medical School of Southeast University, Nanjing, People's Republic of China; [4]Department of Clinical Research Center, The Second Hospital of Nanjing, Nanjing University of Chinese Medicine, Nanjing, People's Republic of China; [5]Nurturing Center of Jiangsu Province for State Laboratory of AI Imaging & Interventional Radiology (Southeast University), Center of Interventional Radiology & Vascular Surgery, Department of Radiology, Medical School, Zhong da Hospital, Southeast University, Nanjing, Jiangsu People's Republic of China

*These authors contributed equally to this work

Correspondence: Chunmei Hu, Department of Tuberculosis, the Second Hospital of Nanjing, Affiliated to Nanjing University of Chinese Medicine, Zhongfu Road 1-1, Yijiangmen Street, Nanjing, Jiangsu Province, 210009, People's Republic of China, Email njyy003@njucm.edu.cn

International Journal of Nanomedicine downloaded from https://www.dovepress.com/
For personal use only.

Purpose: Treatment for bone and joint tuberculosis (BJTB) is challenging due to its refractory and recurrent nature. This study aimed to develop a bioimplantable scaffold with osteoinductive and antituberculosis characteristics to treat BJTB.

Methods: This scaffold is built on oxidized hyaluronic acid and carboxymethyl chitosan hydrogel mixed with hydroxyapatite as a bone tissue engineered material. In order to make the scaffold have the biological activity of promoting tissue repair, the engineered exosomes (Exo_{eng}) were added innovatively. In addition, drug-loaded liposomes equipped with an aldehyde group on the surface are cross-linked with the amine group of the hydrogel skeleton to participate in the Schiff base reaction.

Results: The designed scaffold has characteristics of self-healing and injectability exhibit excellent anti-tuberculosis and promoting bone repair activities. Exo_{eng} strongly stimulates cellular angiogenesis and osteogenic differentiation. The liposomes coated in hydrogel can release three kinds of anti-tuberculosis drugs smoothly and slowly, achieving a long term anti-tuberculosis.

Conclusion: The composite bio-scaffold shows good tissue repair and long-term anti-tuberculosis abilities, which expected to provide a viable treatment plan for bone-related BJTB.

Keywords: hydrogel scaffolds, engineered exosomes, triple anti-tuberculosis drugs loaded, bone and joint tuberculosis, therapy

Introduction

Tuberculosis (TB) is a public health problem with high morbidity and mortality.[1] Extrapulmonary tuberculosis (EPTB) accounts for approximately 10~20% of all TB cases, with bone and joint tuberculosis (BJTB) being one of the most common forms of EPTB.[2] BJTB can prompt joint destruction, deformity and even paraplegia, causing immense pain and placing a heavy burden on patients.[3] Chemotherapy is used as the basic method for effectively treating BJTB, and to address complications and improve prognosis, surgical removal of TB is important.[4] However, traditional oral drug administration has severe limitations, such as long treatment times, low drug concentrations at the lesion site and a variety of side effects due to severe toxicity. Additionally, after surgical removal of the lesion, the bone defect is too large to heal, which can easily lead to recurrence of the abscess at the lesion site.[5,6] Therefore, it is necessary to construct a local drug delivery system for lesions based on bionic artificial bone composite scaffold materials to treat BJTB.

Received: 21 August 2024
Accepted: 12 December 2024
Published: 31 January 2025

© 2025 Huang et al. This work is published and licensed by Dove Medical Press Limited. The full terms of this license are available at https://www.dovepress.com/terms.php and incorporate the Creative Commons Attribution – Non Commercial (unported, v3.0) License (http://creativecommons.org/licenses/by-nc/3.0/). By accessing the work you hereby accept the Terms. Non-commercial uses of the work are permitted without any further permission from Dove Medical Press Limited, provided the work is properly attributed. For permission for commercial use of this work, please see paragraphs 4.2 and 5 of our Terms (https://www.dovepress.com/terms.php).

Recently, biodegradable materials have attracted much attention for their clinical application potential as scaffolds due to their ability to facilitate rapid localized absorption and be replaced with autologous bone.[7] Compared with covalently crosslinked hydrogels, novel injectable self-healing hydrogels are based on dynamic covalent bonds. These hydrogels can spontaneously and quickly repair damaged structures.[8] By combining the preparation in the sol state, drug loading can be achieved. Upon in vivo injection, the hydrogel formed in situ can achieve sustained release of the loaded content. An injectable maltodextrin-based micelle/hydrogel composite system loaded with simvastatin exhibited bone regeneration properties.[9] A semi-interpenetrating gelatin-based hydrogel incorporating mesoporous silica nanoparticles loaded with rifampicin (RFP) and levofloxacin could maintain the drug concentration for more than 60 days and efficiently inhibit *Mycobacterium tuberculosis*.[10] To promote osteogenesis and reduce the tuberculosis recurrence rate, ideal drug-loaded bone scaffolds should possess bone-inducing characteristics and provide the slow release of long-acting anti-tuberculosis drugs. However, the materials reported in the literature do not fulfill both requirements simultaneously.

Exosomes derived from stem cells are nanosized vesicles (40–150 nm) that can deliver a variety of small biomolecules, including mRNAs, miRNAs, and proteins, to recipient cells.[11,12] Recently, emerging studies have shown that exosomes can be used as a possible alternative to mesenchymal stem cell (MSC) therapy because of their immune tolerance and ability to show biological functions similar to the cells from which they were derived.[13,14] Nevertheless, natural exosomes face challenges such as poor internal circulation stability and insufficient targeting.[15] To address these issues, researchers have begun developing engineered exosomes by employing bioengineering methods and chemical functionalization to enhance exosome quality and customize their applications.[16,17] Wu et al synthesized a new type of exosome derived from bone mesenchymal stem cells (BMSCs) that was stimulated with magnetic nanoparticles (Fe_3O_4 nanoparticles) and a static magnetic field to further enhance the effects of the BMSC-derived exosomes on bone regeneration.[18]

In this research, a sustained release medication strategy that combines TB inhibition with bone induction was investigated. Using oxidized hyaluronic acid (OHA) and carboxymethyl chitosan (CMCS) as precursors, we formed an injectable hydrogel with Schiff base reaction. Nano-hydroxyapatite (nHAP) is incorporated to enhance the mechanical properties of the hydrogel, meanwhile we added engineered exosomes and liposomes containing pyrazinamide (PZA), isoniazid (INH), and RFP. The hydrogel scaffold provides a biocompatible structure for bone regeneration and sustains the release of the loaded anti-tuberculosis drugs from the liposomes, while the engineered exosomes generated by dual stimulation of BMSCs with Fe_3O_4 nanoparticles and an alternating magnetic field (AMF) more potently promote osteogenesis (Scheme 1).

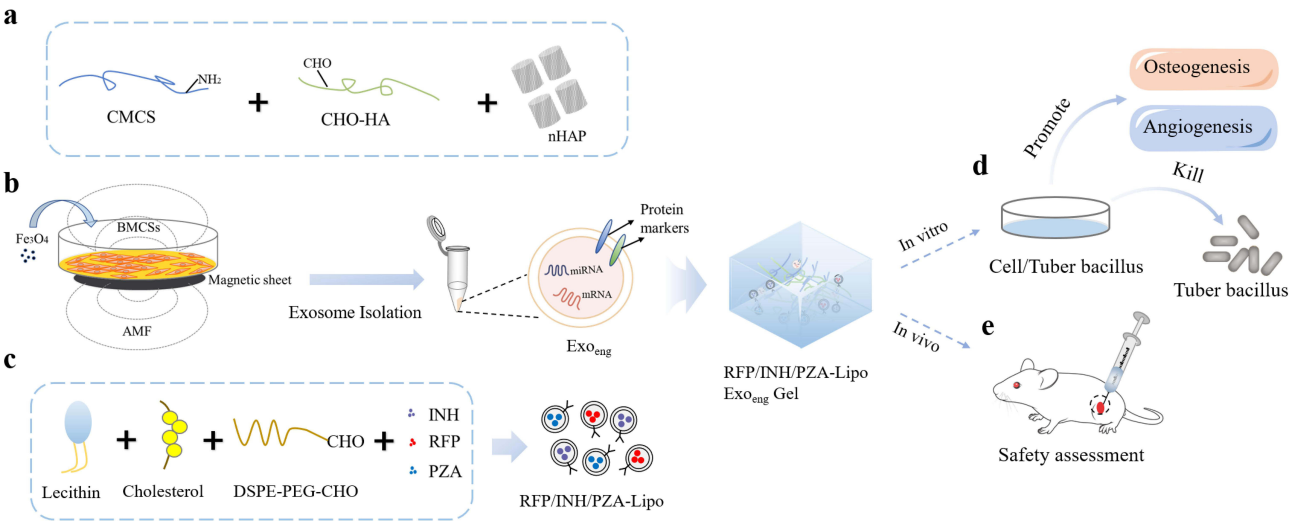

Scheme 1 Illustration for the present study. (**a**) The preparation of OHA/CMCS/HAP hydrogel (Gel). (**b**) The preparation of engineered exosomes (Exo_{eng}). (**c**) The preparation of liposomes loaded with RFP, INH, and PZA (RPF/INH/PZA-Lipo) by means of the film dispersion method. (**d**) In vitro study of the RFP/INH/PZA-Lipo Exo_{eng} Gel including cells culture study and antituber bacillus study. (**e**) In vivo femoral ankles injection of the RFP/INH/PZA-Lipo Exo_{eng} Gel and safety assessment in vivo.

Materials and Methods

Preparation of HA Modified by Aldehyde Groups

OHA was synthesized sequentially by oxidizing HA with sodium periodate.[19] In short, HA aqueous solution (100 mL, 10 mg/mL) was dropped into sodium periodate aqueous solution ($NaIO_4$, 1 mL, 0.5 M), and HA was oxidized with sodium periodate. After stirring for 24 hours, ethylene glycol (1 mL) was added to the stirred solution to stop the reaction. The combined mixture was dialyzed and lyophilized to obtain aldehyde-grafted oxidized HA.[2]

Preparation of Dynamic Hydrogel

Dissolve OHA or CMCS and prepare aqueous solutions with mass concentrations of 2%, 3%, and 4%. In order to improve the mechanical strength of the hydrogel, nHAP was dissolved in CMCS aqueous solution at a mass concentration of 8%.[20] According to the mass concentration after mixing, they are called Gel2%, Gel3%, and Gel4%. Then, two corresponding concentrations were compared at a volume ratio of 1:1 and the solution were mixed by double syringes to obtain dynamic hydrogels.

Hydrogel Characterization

The chemical structures of polymers and hydrogels were characterized using Fourier transform infrared (FTIR) spectra and were analyzed with a SHIMADZU IRAffinity-1S within the range of 4000–600 cm^{-1}. The gelation time of the hydrogel was determined using the vessel inversion method. The storage modulus (G') and loss modulus (G") of the three hydrogels were measured using a rheometer (Anton Paar MCR302, Austria). The swelling ratio for the three hydrogels was calculated using the formula: Swelling ratio = (Wt-W0)/W0 × 100%. The hydrogels were immersed in PBS at 37°C to determine the degradation rate. The degradation rate was calculated using the formula: Degradation rate = (W0-W1)/W0 × 100%.[21] The self-healing properties of the hydrogels were initially evaluated on a macroscopic scale. In short, a hydrogel disk was cut into two pieces using a razor blade. The gel pieces were then reassembled and allowed to self-heal for 2 hours under ambient conditions without any further treatment. This was followed by manual raising, and pictures were taken. The hydrogel morphology was characterized using scanning electron microscopy (SEM). The lyophilized hydrogels were placed on platform, sputter-coated with gold and examined under the Hitachi S-4800. SEM images were obtained.

Cell Culture and Reagents

We extracted BMSCs from the bone marrow of 3–4 weeks Sprague-Dawley rats. In short, rat femurs and tibias were exposed and subsequently flushed with culture medium to collect rBMSCs. The isolated cells were then grown in DMEM/F12 with 10% FBS. Only cells between 2 and 5 passages were used for experimentation.

Human umbilical vein endothelial cells (HUVECs) were obtained from Zhong Qiao Xin Zhou Biotechnology Co., Ltd, (Shanghai, China). They were grown in endothelial cell special medium. Culture medium was replaced every 3 days.

L929 cells (Zhong Qiao Xin Zhou Biotechnology Co., Ltd, Shanghai, China) were cultured under standard culture conditions in Roswell Park Memorial Institute (RPMI) 1640 medium with 10% FBS. Replace the entire culture medium every two days.

All cells were cultivated at 37°C with 5% CO_2 environment. Most cell culture media and reagents were purchased from Gibco (Carlsbad, CA, USA). Cell culture plates were obtained from NEST Biotechnology Co., Ltd. (Wuxi, China).

Magnetic Fe_3O_4 and AMF

Fe_3O_4 nanoparticles (3 mg/mL) were added to the culture medium at a final concentration of 25 μg/mL.[22] The electromagnetic field generator (Derived Technology Co., Ltd, Hunan, China) consists of a sinusoidal variable frequency AC power supply and a pair of Helmholtz coils. Separate cultures of BMSCs were cultured in medium alone or medium containing Fe_3O_4 nanoparticles at various concentrations with or without exposure to an AMF. Magnetic field groups were exposed to AMF (50 hz frequency) for one hour each day under intensities of 3mT.[23]

 https://doi.org/10.2147/IJN.S480288

Isolation and Purification of Exosomes

To improve the purity of rBMSC-received exosomes, FBS was centrifuged that spins something at a high speed at 110,000×g for 70 mins to remove endogenous exosomes before it was used for cell culture at first. We separated exosomes according to our before-published rules of conduct.[24] The supernatant was collected using centrifugation (300×g for 10min, 2000×g for 10min, and 10,000×g for 30min at 4°C) to remove cell many broken pieces of something destroyed. The suspension was centrifuged at 110,000×g and 4°C for 70 mins. Then, the exosomes were washed in PBS, and ultra-centrifuged again. In the end, the exosomes were resuspended in PBS and stored at −80°C.

Characterization and Release Profile of Exosomes

The exosomes were carefully studied by transmission electron microscopy (TEM, Hitachi, Tokyo, Japan), and nano-particles Tracking Analysis (NTA, Particle Metrix, Germany) and their characteristic molecules, such as CD81, CD9, TSG101, and Calnexin, were identified by Western blotting.

The hydrogel preparation steps are the same as above, but we use exosome-containing PBS to dissolve OHA. BCA protein test was used to detect the release of exosomes in composite hydrogels. Briefly, 250 μL of a 1 μg/μL exosomes were used to prepare the hydrogel system. After that, the Gel system was placed in PBS at 37°C, and the supernatant was continuously collected for 14 days. The amounts of exosomes liberated was calculated and the release curve was plotted.

Cell Toxicity Evaluation in vitro

The hydrogel with exosomes should be placed in a 24-well plate, with 200 μL of Gel per well. Then, add 2 mL of DMEM/F12 complete culture medium separately and place the plate in a 5% CO_2 cell incubator at 37 °C for 48 hours to prepare the extract. rBMSCs and HUVECs were separately cultured at a ratio of 2×10^3 cells/mL and then inoculated into 96 well plates for 24 h. The initial culture medium was aspirated, and 200 μL of hydrogel extract was added to each well. After 48h of culturing, 100 μL of cell culture medium and 10 μL of CCK-8 reagent were added to each well and the cells were incubated for 2 h. At last, the absorbance of each well solution was measured at a 450 nm wavelength using an enzyme microplate reader, and the cell activity percentage was calculated following the provided instructions.[25]

Scratch Wound and Tube Formation Assay

The $OHA_3/CMCS_3/HAP_8$ composite hydrogel (Gel) with Exo (40 μg) was used for experiments. After covering HUVECs with 6 well plates, the monolayer of cells cultured in the plates was scratched using sterile 200 μL pipette tips to create linear scratches. The cells were then cultured in 1% serum medium or hydrogel extracts prepared above for 24 h, and imaged by an inverted microscope. Matrigel (Beyotime Biotechnology, China) was pipetted onto 96 well plates (50 μL Matrigel per well) and allowed to a 60 min solidify at 37 °C. Approximately, 100 μL of cell suspension with 3×10^4 HUVECs was seeded onto a Matrigel pretreated plates with hydrogel extracts. After 8 h incubation period, the newly formed tubular structures were imaged, and the length of capillaries, the number of junctions, and nodes were measured and counted. All consumables that came into contact with the Matrigel were pre-cooled before use.

Alkaline Phosphatase and Alizarin Red Staining

The preparation steps for the hydrogel extract were the same as above, except the culture medium was replaced with an osteogenic induction medium. rBMSCs at a density of 2×10^4 per milliliter are inoculated into a 12 well plate. The medium was replaced with the prepared hydrogel extract when the cells adhered to the wall. After 7 days of osteogenic induction, the cells were fixed with 4% paraformaldehyde and washed three times with ddH_2O. At room temperature with an alkaline phosphatase staining reagent for 30 minutes, the samples were observed under an inverted microscope. In addition, the alkaline phosphatase activity assay was performed by combining 50 μL of sample with 50 μL of the colorimetric substrate para-nitrophenyl phosphate and detecting the absorbance at 405 nm. The alkaline phosphatase activity of samples was calculated by comparing it to a known concentration of alkaline phosphatase.

After 14 days of osteogenic induction, Alizarin Red staining was performed for 30 minutes to detect intracellular calcium deposition. Then, 10% cetyl pyridinium chloride was incorporated to dissolve the stained calcium nodules in the

mineralized nodules for further semi-quantitative analysis. Measure the content of sample solution at a 450 nm using an enzyme microplate reader.

Real-Time PCR Analysis

The genes associated with vascular and osteogenic differentiation were assessed using real-time quantitative polymerase chain reaction. Total RNA was extracted from cells using Trizol and then reverse-transcribed into cDNA using a reagent kit according to the instructions. The mRNA expression was evaluated by qRT-PCR using SYBR Green mRNA analysis kit and ABI StepOne^{TM} Real-time PCR system. We normalize mRNA expression levels using the GAPDH method and perform relative quantification using $2^{-\Delta\Delta Ct}$ method. The qRT-PCR primer sequences are provided in Table S1 of the attachment. All reagents were purchased from Vazyme Biotech Co., Ltd, China.

Preparation and Characterization of Liposomes

Liposomes and drug-loaded liposomes were prepared utilizing the thin film hydration method.[26] Egg yolk lecithin, cholesterol, and DSPE-PEG-CHO were combined in a weight ratio of 10:1:1 and dissolved in a mixture of chloroform and methanol with a 3:2 (v/v) ratio. The organic solvent was eliminated through rotary evaporation, resulting in the consistent formation of a film. Following this, 10 mL of distilled water was introduced to fully hydrate the formed film, and the liposome underwent ultrasonication in an ice bath for 30 mins (ultrasonication for 5 sec, with an interval of 5 sec) to achieve the free-loaded liposome. The fat-soluble drug (RFP) was dissolved in combination with cholesterol, and the water-soluble drugs (INH and PZA) were incorporated during the hydration process.

The specimens were subjected to re-staining with 2% phosphotungstic acid, and the morphology of the liposomes was examined using transmission electron microscopy (TEM). The particle size, polydispersity index (PDI) of the samples were analyzed by Dynamic Light Scattering (DLS, NS-90Z, Omec Instrument Co., Ltd, Zhuhai, China). The drug loading rate of the drug-carrying liposomes was evaluated through ultrafiltration centrifugation. Ultrafiltration centrifuge tubes (Merck Millipore, 30 kDa cutoff, China) were employed to accommodate 3 mL of liposomes, which were subsequently centrifuged at 7500 g/min for 10 min to assess their drug loading efficiency. The drug concentrations of RFP, INH, and PZA in the solution were determined by UV spectrophotometer at wavelengths of 473 nm, 263 nm, and 269 nm, respectively. The drug loading capacity (LC%) is calculated using the following formula:[27] LC%= $Drug_{loaded}$ /$Liposome_{total}$ × 100%. Where "$Drug_{loaded}$" represents the weight of the encapsulated drug in the liposome, and "$Liposome_{total}$" denotes the total weight of the liposome including the drug.

Drug Release Profile in vitro

The cumulative drug release profile was determined using a method that has been previously reported in the literature.[10] The drug-loaded liposomes were encapsulated in Exo_{eng} hydrogel and then introduced into 2 mL of release medium (PBS-pH 7.4) within a dialysis bag (8 kDa-14 kDa, Solarbio). The dialysis bag was immersed in a 50 mL centrifuge tube with 5 mL of release medium and subjected to agitation at a speed of 100 rpm at a stable temperature of 37°C. The outer solution was replaced at specified intervals over 28 days, with each replacement consisting of 5 mL of fresh-release medium. The UV spectrophotometer identified the emission of RFP, INH, and PZA at wavelengths of 473 nm, 263 nm, and 269 nm, respectively, and the cumulative drug release data were graphed against time.

Antimicrobial Assay

The minimum inhibitory concentration[28] of *Mycobacterium tuberculosis* (H37Rv) was established through the dilution method. 100 μL of 7H9 and 100 μL of the drug-loaded Exo_{eng} hydrogel degradation solution was mixed in a 96 well plate, and the resultant mixture was then diluted to generate 10 columns with a gradient. RFP and INH concentrations (0.0625, 0.125, 0.25, 0.5, 1, 2, 4, 8, 16, 32 μg/mL) and PZA (1. 171,875, 2.34375, 4.6875, 9.375, 18.75, 37.5, 75, 150, and 300 μg/mL) were each added to four replicate wells within their respective groups. Subsequently, 100 μL of bacterial suspension (MCF = 0.05) was added to each well, except for 12 columns without drug and bacteria, only with 7H9 medium. The culture should be maintained for 3–4 weeks.

The bacteriostatic properties of both a simple hydrogel and a drug-loaded hydrogel were evaluated using the smear plate method. Initially, the release solution of both hydrogels for 7, 14, 21, and 28 days was collected, filtered through a 0.22 μm microporous filter membrane, and subsequently stored. The H37Rv bacterial suspension was diluted to achieve a concentration MCF of 1.0. Subsequently, 100 μL was transferred into 1.5 mL EP tubes, and both negative and positive controls were established. Transfer 100 μL of the release solution collected on days 7, 14, 21, and 28 into the EP tube containing the bacterial solution. Subsequently, the solution should be removed after being subjected to culture for 4 h at 37°C in a warm box. Gradient dilutions were prepared, and 100 μL of bacterial solutions with gradients of 10^{-3}, 10^{-4}, 10^{-5}, and 10^{-6} were used to inoculate the plates, with two replicates for each dilution.

Biosafety in vivo

Sprague-Dawley rats, 8 weeks old and weighing 250–300 g, were obtained from Qing long shan Animal Farm, Nanjing, China. Rats were randomly divided into three groups (Control: without anything; Blank gel: the hydrogel without exosomes or drugs; RFP/INH/PZA-Lipo Exo_{eng} Gel) to evaluate the in vivo safety of scaffolds. The rat underwent surgical exposure to create a cylindrical bone defect measuring 3 mm and 3 mm using a saline-flushed drill. Following this, a hydrogel scaffold was implanted into the defect, the subcutaneous tissue was sutured, and the skin was closed with sutures. Three rats were selected randomly at 1, 2, and 4 weeks postoperatively. Blood samples were obtained for biochemical analysis, and the heart, liver, spleen, lungs, and kidneys were extracted for histological examination. Appropriate measures were taken during experimental procedures to minimize animal suffering and reduce the number of animals used. Measurements were taken once animal surgeries were stabilized, and concluded with euthanasia of each animal.

Statistical Analysis

The data present the mean ± standard deviation (SD) of three independent experiments and underwent analysis using GraphPad Prism Version 9.0 software (GraphPad Software, Inc., San Diego, CA, USA). Disparities were assessed by means of the *t*-test or one-way analysis of variance (ANOVA). $p < 0.05$ was considered as statistically significant.

Results and Discussion

Fabrication and Characterization of the Hydrogel Scaffold

By utilizing a Schiff base reaction between OHA and CMCS, an injectable hydrogel with self-healing capabilities was created. First, sodium periodate, as an oxidizing agent, was used to target the nearby hydroxyl groups on the sugar ring to generate dialdehydes, which caused the sugar ring to open and give rise to dialdehyde derivatives.[19] Figure 1a shows the chemical structures of OHA and CMCS. OHA has an oxidation degree of 48.9%, as determined by the alkali consumption technique.[29] The Schiff base reaction between the amino groups of CMCS and the aldehyde groups of OHA is thought to be the mechanism of gelation.[15] In the Fourier transform infrared (FTIR) spectrum (Figure 1b), a new peak at 1727 cm^{-1}, assigned to C=O, appeared (compared to the spectrum of HA), suggesting the formation of aldehyde groups in OHA. In the OHA/CMCS hydrogel spectrum, a distinct peak at 1621 cm^{-1} was observed, corresponding to the characteristic band of an imine (C=N).[30] This finding confirms the occurrence of the Schiff base reaction between OHA and CMCS. The gelation time of the hydrogel was evaluated via the vial inversion method (Figure S1). Higher concentrations cause the hydrogels to gel more quickly, as shown in Figure 1c. Furthermore, when manufactured at a concentration of 4% (w/w, Gel 4%), the OHA/CMCS/HAP hydrogel (Gel) efficiently cured in 38s. Hydrogels must be able to flow over time to be injectable, which stops leakage from the injection site and makes in vivo administration much more convenient.[13,31,32] The stability of the three-dimensional network in the hydrogel system was significant, possibly because the storage modulus (G′) of each hydrogel was greater than the loss modulus (G″) within the frequency range of 1–100 hz (Figure 1d). The three categories of hydrogels exhibit remarkable stability across a broad spectrum of strains, particularly within the range of strains tolerated by bone (<7%,[33] Figure 1e). As illustrated in Figure 1f, the viscosities of the hydrogels prepared in this study decreased significantly with increasing shear rate after 0.05 s^{-1}, indicating the characteristic shear-thinning behavior that facilitates the ease of injection. Typically, the water absorption

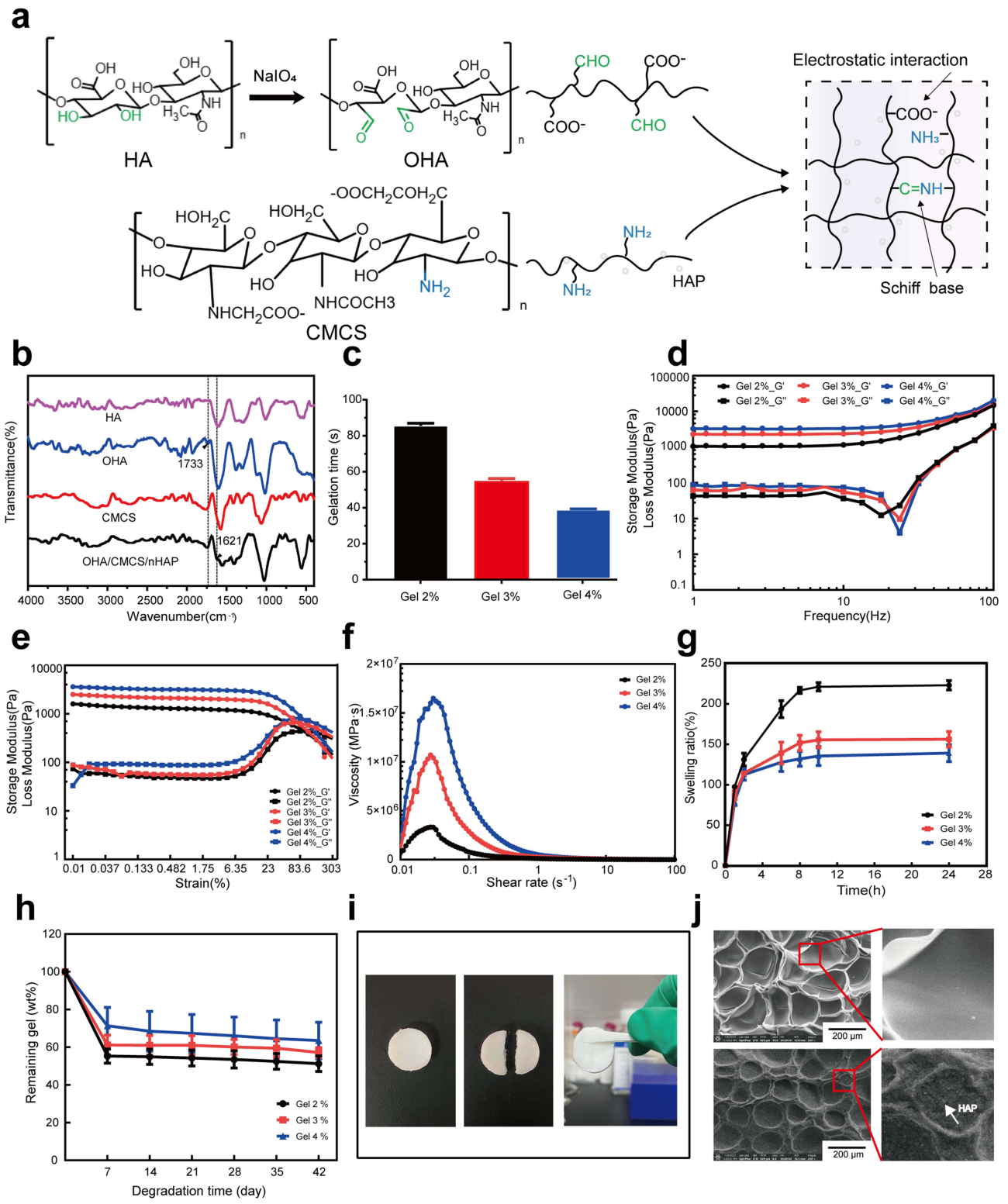

Figure 1 (**a**) Synthesis of OHA and OHA/ CMCS/ HAP hydrogel. (**b**) FTIR spectra of HA, OHA, CMCS and OHA/CMCS/HAP hydrogel. (**c**) Gelation time of hydrogel concentration increases from 2% to 4%(w/v) (n=3). (**d**) Frequency-sweep measurements of various concentration hydrogel. (**e**) Rheological analysis of various concentration hydrogel in a strain-sweep mode. (**f**) Shear-thinning behavior of various concentration hydrogel. (**g**) Swelling ratio of various concentration hydrogel. (**h**) Degradation of various concentration hydrogel. (**i**) The macroscopic observation of self-healing property. (**j**) SEM images of $OHA_3/CMCS_3$ hydrogel and $OHA_3/CMCS_3/HAP_8$ hydrogel. Scale bars are 200 μm.

https://doi.org/10.2147/IJN.S480288

capacity is assessed by measuring hydrogel swelling. The hydrogel with a concentration of 2% (Gel 2%) displayed a greater swelling rate than Gel 3% and Gel 4%, as demonstrated in Figure 1g. Then, the in vitro biodegradation of the gels was investigated. Figure 1h shows that the hydrogel degradation curve is consistent with the properties of most hydrogels published previously.[31,34] The decrease in mass during the initial 7-day period could be attributed to hydrolysis of the hydrogel.[21] Subsequently, there was a gradual decrease in mass over the subsequent days, possibly due to the degradation of the crosslinked regions, resulting in a residual Gel 3% weight of 57% after 42 days. We chose Gel 3% for subsequent experiments due to its moderate swelling ratio and slow degradation rate, which facilitates nutrient absorption and hydrogel stabilization.

The self-healing ability of Gel was observed from a macroscopic perspective. As depicted in Figure 1i, the hydrogel demonstrated self-healing properties when divided into two parts and repositioned, merging into a single hydrogel within 2 h. Despite visibly making a cut line, the hydrogel remained intact and could be lifted with forceps. The morphologies of the hydrogels obtained from OHA/CMCS and Gel were observed using scanning electron microscopy (SEM) (Figure 1j). The OHA/CMCS hydrogel had a porous structure with smooth walls and an aperture size of 200–300 μm, while Gel had a large amount of HAP on the pore wall. This was due to the addition of HAP, which resulted in a much denser network structure. The very porous nature of both types of hydrogels with pore sizes exceeding 100 μm promoted cell proliferation inside the scaffold.[35] Therefore, Gel is a potential material for tissue repair and regeneration because of its remarkable stability, injectability, and capacity for self-repair, which will provide target tissues with steady support.

Exosomal Characterization, Release and Cytocompatibility in vitro

The obtained rat BMSCs (rBMSCs) were long and shuttle shaped under a microscope. By day 7, they had grown quickly with a whirling arrangement (Figure S2a). The induced differentiation of rBMSCs showed that they could differentiate into osteoblasts and adipocytes (Figure S2b). The rBMSCs surface markers were analyzed by flow cytometry, as shown in Figure S2c. Both CD29 (99.6%) and CD90 (99.4%) were expressed, while the expression of CD45 (1.33%) was low, consistent with the BMSC phenotype.[36,37] These findings demonstrated that rBMSCs were extracted successfully. To extract exosomes originating from rBMSCs, the conditioned media was subjected to differential centrifugation. The four types of exosomes were characterized and quantified, and the NTA results indicated that the four groups of exosomes had particle sizes predominantly in the range of 50–150 nm (Figure 2a). Transmission electron microscopy (TEM) analysis revealed that the exosomes derived from rBMSCs were round or saucer shaped (Figure 2b), consistent with previously reported findings.[11,38,39] Western blotting revealed that rBMSC-Exos expressed the specific biomarkers CD81, CD9, and TSG101 and did not express Calnexin (Figure 2c). These data prove the successful isolation of engineered exosomes from the rBMSCs culture supernatant. Exosomes were encapsulated in Gel3%, and their release was detected using a BCA protein kit. Figure 2d shows that exosome release was complete after 11 days. The extract of the hydrogel encapsulating exosomes was collected and cocultured with rBMSCs and HUVECs for 48 h. Figure 2e shows that Exo Gel exhibited good biocompatibility, with these two types of cells showing viability percentages of 94.16 ± 2.86% and 97.41 ± 0.73%, respectively. Several studies have demonstrated that hydrogels can serve as effective carriers for the slow release of exosomes while preserving their biological activity. For instance, pure polymer lactic acid hydroxyacetic acid copolymerhas (PLGA) been shown to encapsulate extracellular vesicles, which were completely released within 3 days. In a study by Li et al[40] the modification of PLGA scaffolds with polydopamine (pDA) resulted in 30% of the residual extracellular vesicles remaining after eight days of encapsulated release, thereby prolonging the secretion process. In our study, exosomes were continuously released from the hydrogel system over a period of 11 days, indicating a comparable sustained release duration. The release of exosomes with a various time was attributed to the following aspects: First, variations in hydrogel composition, especially the molecular weight. Such as increasing PEG molecular weight and decreasing PEG weight percentage increases hydrogel mesh size, leading to more rapid release.[41] Second, the exosomes were loaded in hydrogel scaffold with physical crosslinking, which will be disrupt by release buffer (PBS) leading to the fast release of exosomes. Moreover, the degradation rate of hydrogel affected the release rate of exosomes from the hydrogel.[42] In initial stage, hydrogel degraded for hydrolysis result in the exosomes released from the hydrogel.

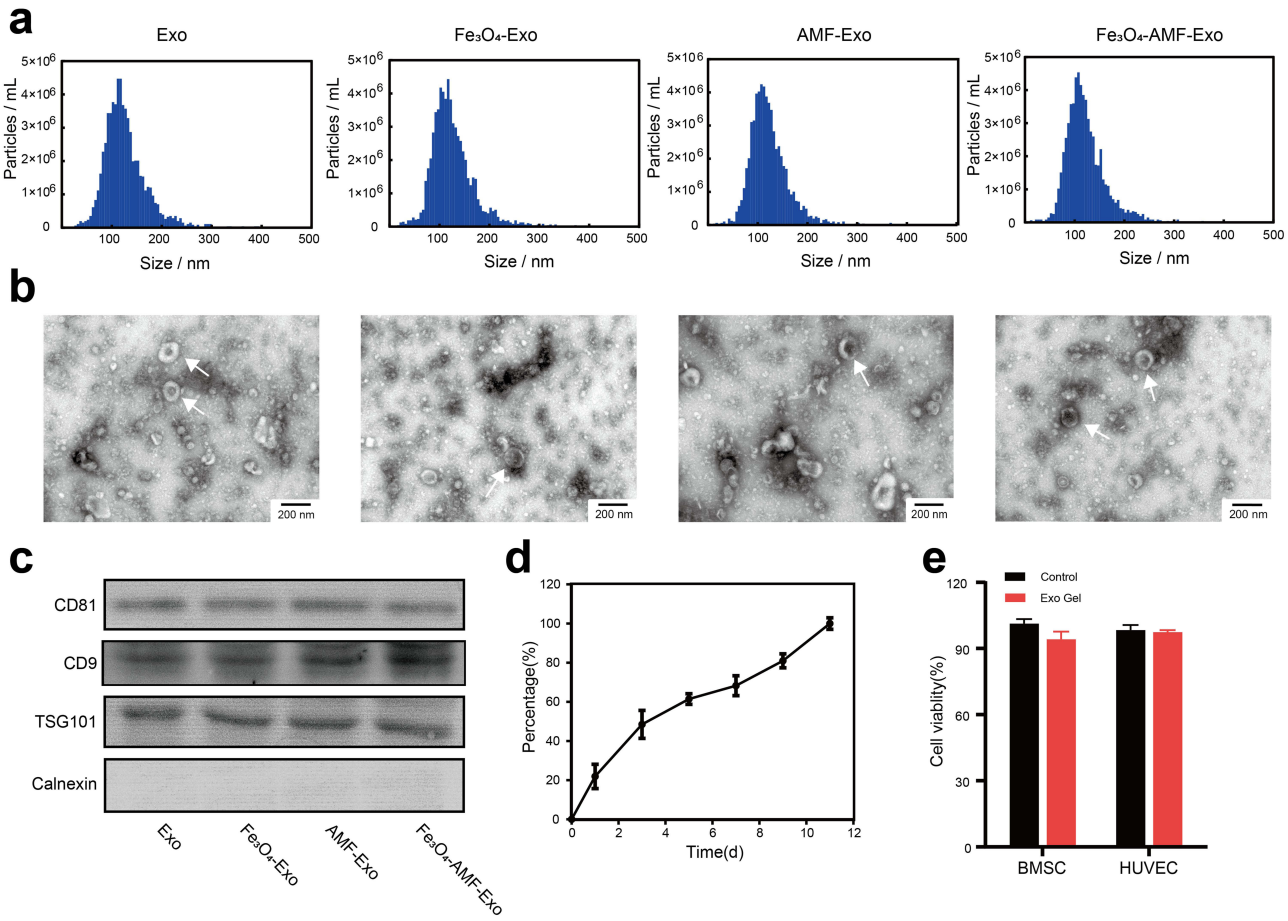

Figure 2 (**a**) NTA analysis of four types of exosomes. (**b**) Morphology of four types of exosomes under TEM, the white arrows indicate exosomes. Scale bars are 200 nm. (**c**) Western blotting analysis of exosomal proteins CD81, CD9, TSG101 and the negative marker Calnexin. (**d**) Release profiles of exosomes from $OHA_3/CMCS_3/HAP_8$ hydrogel. (**e**) Effect of $OHA_3/CMCS_3/HAP_8$ hydrogel extracts on cell viability measured by CCK8 assay.

Angiogenic Effect of rBMSC-Exos in vitro

To evaluate the potential of using Gel loaded with engineered exosomes to enhance the migration of HUVECs, a time-dependent assay (0–24 h) was conducted. As shown in Figure 3a and c, HUVECs cocultured with exosome-loaded Gel extracts migrated significantly faster than those cocultured with Gel extracts after 24 h of incubation ($p < 0.01$). Additionally, the cells in the Fe_3O_4-AMF-Exo Gel group exhibited faster migration than those in the other three groups ($p < 0.001$). MSC-derived exosomes have been shown to accelerate wound healing.[43–45] Furthermore, hydrogel-exosome complexes have a synergistic effect compared to exosome therapy alone,[46] as the hydrogel enhances the persistence and stability of the exosomes. The Matrigel method was used to detect the impact of the Gel loaded with exosomes on the ability of HUVECs to form an endothelial cell network. The HUVECs on the matrix gel formed small tubular structures after 8 h of incubation (Figure 3b). Compared with the Gel group, the exosome-containing hydrogel group exhibited greater tubular network formation. Among the hydrogels containing exosomes, the Fe_3O_4-AMF-Exo group had a greater ability to promote tube formation. Further analyses of tube length, connections, and node volume confirmed the phenomenon mentioned above (Figure 3d-f), indicating that Fe_3O_4 nanoparticles, when combined with a magnetic field, can stimulate exosomes and facilitate angiogenesis.[18] Next, we examined the expression profiles of genes associated with angiogenesis (HIF-1α, VEGF, and ANG-1) in HUVECs cocultured with hydrogel extracts for 4 days. The results demonstrated the greatest upregulation of HIF-1α, VEGF, and ANG-1 in the Fe_3O_4-AMF-Exo Gel group (Figure 3g-i). Angiogenesis refers to the physiological process through which new blood vessels emerge from the pre-existing vascular network. This dynamic process is driven by angiogenic activity, which involves a range of cellular functions and molecular mechanisms, including the proliferation, migration, and lumen formation of endothelial

https://doi.org/10.2147/IJN.S480288

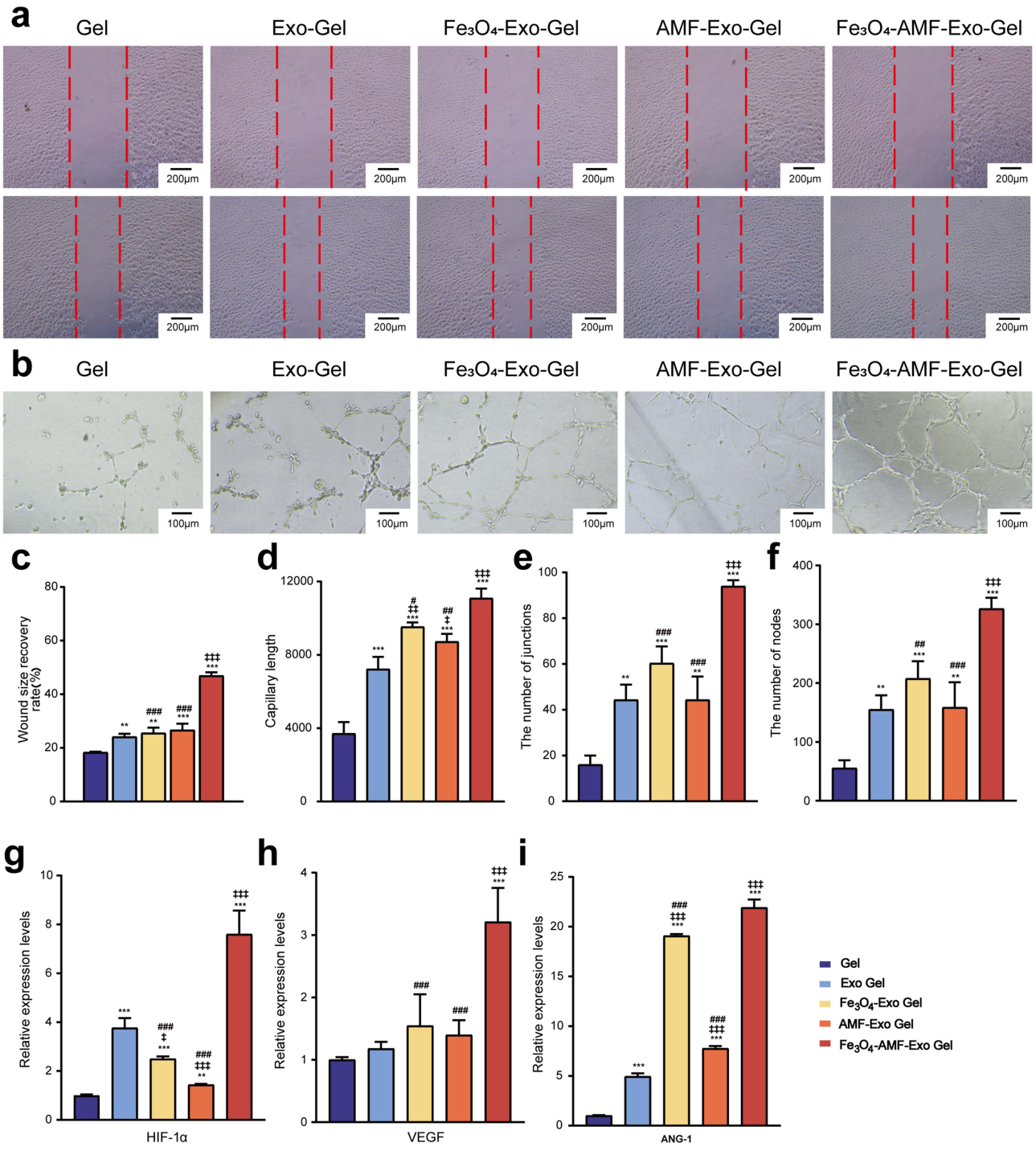

Figure 3 (**a**) Assessment of the migratory activity of HUVECs in coculture for 24 h by scratch wound assay (scale bars are 200 μm), the red dashed lines are the edges of the cell migration. (**b**) Observation of tube formation under the inverted light microscopy in coculture for 8 h. Scale bars are 100 μm. (**c**) Semi-quantitative results of the wound recovery rate. (**d-f**) Semi-quantitative results of tube formation assays. (**g-i**) mRNA expression levels of HIF-1α, VEGF, and ANG-1. Data are shown as mean ± standard error (n=3). (**p<0.01, ***p<0.001 vs Gel group. ‡ p < 0.05, ‡‡p < 0.01, ‡‡‡p < 0.001 vs the Exo Gel group. #p < 0.05, ##p < 0.01, ###p < 0.001 vs the Fe_3O_4-AMF-Exo Gel group).

cells.[47,48] The results of the above in vitro experiments showed that the stimulation of rBMSC-derived exosomes with nano-Fe_3O_4 and an AMF activated a series of angiogenic responses, including migration and angiogenic activity, in HUVECs, and these kinds of exosomes further enhanced the angiogenic capacity of HUVECs.

Osteogenic Differentiation of rBMSC-Exos in vitro

In addition to good angiogenic ability, the osteogenic differentiation of cells is crucial for effective bone tissue engineering implants.[49] BMSCs have the potential to differentiate into osteoblasts, which is an important part in bone defect repair. During this differentiation process, the numbers of calcium nodules and alkaline phosphatase expression on the cell surface will increase, and related mRNA levels will also rise.[50] As shown in Figure 4a, cells treated with hydrogel extracts containing four different types of exosomes exhibited more intense ALP staining than the cells in the Gel group. Quantitative analysis of ALP activity indicated that the corresponding exosome groups had significant osteogenic effects, with the Fe_3O_4-AMF-Exo Gel demonstrating the greatest effect among them (Figure 4c). Osteogenic differentiation is characterized by calcium deposition, which can be illustrated by alizarin red (ARS)

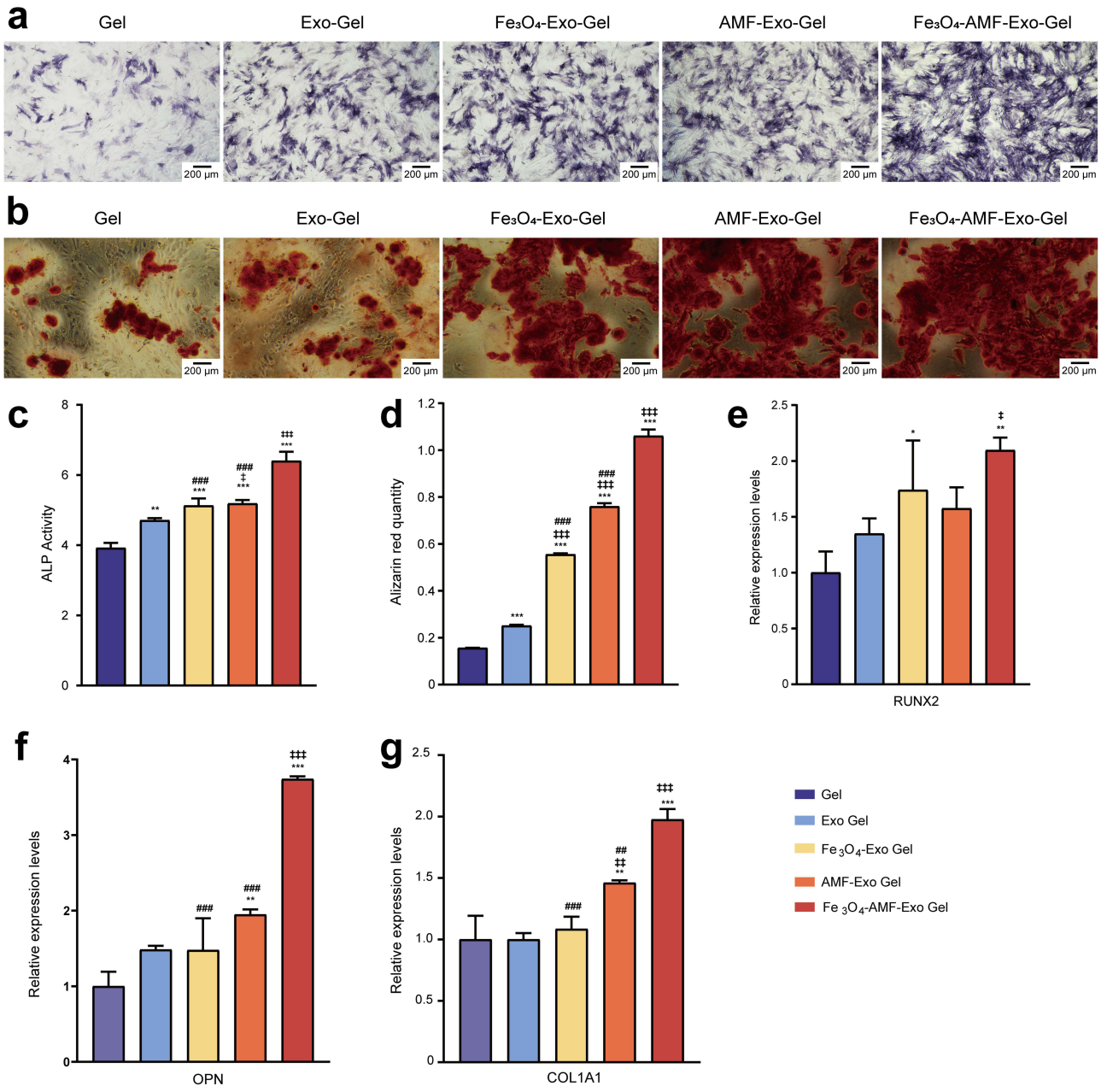

Figure 4 (**a**) Alkaline phosphatase staining (scale bars are 200 μm). (**b**) Alizarin red staining (scale bars are 200 μm). (**c**) semi-quantitative results in coculture for 7days. (**d**) quantitative results in coculture for 14 days. (**e-g**) mRNA expression levels of RUNX2, OPN, and COL1A1. Data are shown as mean ± standard error (n=3). (*p<0.05, **p<0.01, ***p<0.001 vs Gel group. ‡p < 0.05, ‡‡p < 0.01, ‡‡‡p < 0.001 vs Exo Gel group. ##p < 0.01, ###p < 0.001 vs Fe_3O_4-AMF-Exo Gel group).

https://doi.org/10.2147/IJN.S480288

staining.[51] To prepare for in vivo application, we assessed the effect of the composite hydrogels on the osteogenic differentiation of BMSCs. ARS staining after coculture with the hydrogel extracts from each group for 14 days revealed strong staining in the Fe_3O_4-Exo Gel, AMF-Exo Gel, and Fe_3O_4-AMF-Exo Gel groups, while calcium nodule staining in the Gel and Exo Gel groups was limited (Figure 4b). Subsequently, quantitative analysis of the ARS staining results revealed that the Exo Gel, Fe_3O_4-Exo Gel, AMF-Exo Gel, and Fe_3O_4-AMF-Exo Gel groups exhibited significantly more calcium deposits than the Gel group. Moreover, the absorbance of the Fe_3O_4-AMF Exo Gel group was significantly greater than that of the other exosome groups (Figure 4d). To validate the experimental findings, we assessed the expression of osteogenic differentiation genes, including RUNX2, OPN, and COL1A1, via RT–qPCR. The results showed that the expression of pertinent osteogenic genes was significantly upregulated in the Fe_3O_4-AMF-Exo Gel group compared to the other groups (Figure 4e-g). This finding suggested that the capacity of Fe_3O_4-AMF-Exo Gel to enhance the osteogenic differentiation of rBMSCs was greater than that of the other treatments. Numerous studies have demonstrated that Fe_3O_4 nanoparticles and magnetic fields can facilitate tissue repair.[52,53] In general, natural exosomes can specifically target cells and tissue. Numerous studies have shown that Exos can effectively promote the repair and regeneration of bone defects.[54,55] However, the function of natural Exos still cannot meet clinical needs.[56,57] Significantly, External stimuli can modulate the physiological state of the parental cell, thereby affecting the biological function of the exosomes it produces. A research showed that low-intensity pulsed ultrasound enhanced the promoting effect of human BMSC-derived exosomes on cartilage regeneration.[58] Hypoxia preconditioning enhanced the effect of exosomes on bone fracture healing as well as increased the release of exosomes.[59] Therefore, researchers are focusing to develop engineering exosomes by pretreating parental cells for better innate activity of exosomes. Magnetic nanoparticles, such as γ-Fe_2O_3 and Fe_3O_4, have demonstrated the ability to enhance osteogenesis and angiogenesis, whether in the presence or absence of a magnetic field.[60] The FDA has approved low-dose magnetic nanoparticles for iron deficiency anemia.[61] Furthermore, AMF, known as a simple and non-invasive therapy, have positive on MSCs and show capabilities of pro-angiogenesis.[62] To further amplify the osteogenic effect of exosomes derived from rBMSCs, engineered exosomes were obtained by stimulating BMSCs with Fe_3O_4, AMF, and a combination of both Fe_3O_4 and AMF. Recent researchers have combined MSC-Exos with hydrogel materials that have good biocompatibility and resorption characteristics to prepare tissue engineering scaffolds suitable for bone tissue reconstruction.[63–66] Therefore, here engineered exosomes were introduced into Gel. The addition of engineered exosomes to scaffold promoted osteogenesis seeded with rBMSCs, particularly with the Fe_3O_4-AMF-Exo. Although engineered exosome-based therapeutics have demonstrated success in numerous studies, several hurdles remain before they can be tested in the clinic.[67,68] This includes issues such as ensuring consistent quality, controlling the engineering process to avoid batch - to - batch variability, and meeting regulatory requirements for therapeutic use.

Liposome Characterization and Release Profile

TEM images of the empty liposomes and RFP-loaded liposomes showed that the liposomes were elliptical or spherical (Figure 5a; the other liposomes are shown in Figure S3). This result is similar to that previously reported for drug-loaded liposomes.[69–71] The average particle size of the empty liposomes was approximately 200 nm. The particle size images of the RFP, INH, and PZA liposomes showed a slight shift to the right when compared to blank liposomes, suggesting that the incorporation of the drug into the liposomes led to an increase in the particle size of the liposomes (Figure 5b). To evaluate the drug release properties, we collected the drug-loaded Exo_{eng} Gel degradation solution over a few days. As shown in Figure 5c-e, three medications were released rapidly during the first 14 days. Subsequent to the initial fast drug release, the drug release became sustained and gentle from day 14 to day 28. Compared with the quick release of non-liposome group, the liposome-contained scaffold can better meet the long-term anti-tuberculosis treatment. A sustained release period of up to 28 days was observed for RFP concentrations above the MIC (0.06–0.25 μg/mL[72]) and INH concentrations above the MIC (0.03–6.25 μg/mL[73]). The MIC of PZA was 6.2–50 μg/mL at pH 5.5.[74] On day 28, the concentration of PZA used was 6.5 μg/mL, which is expected to effectively inhibit bacterial growth in vivo. Combining RFP, INH, and PZA to treat tuberculosis could effectively reduce the incidence of drug resistance in *Mycobacterium* tuberculosis.[75] Previous studies have primarily focused on using one or two anti-tuberculosis drugs in conjunction with biomimetic scaffolds, while fewer studies have examined the simultaneous use of a triple-drug regimen.[6,76] In this study,

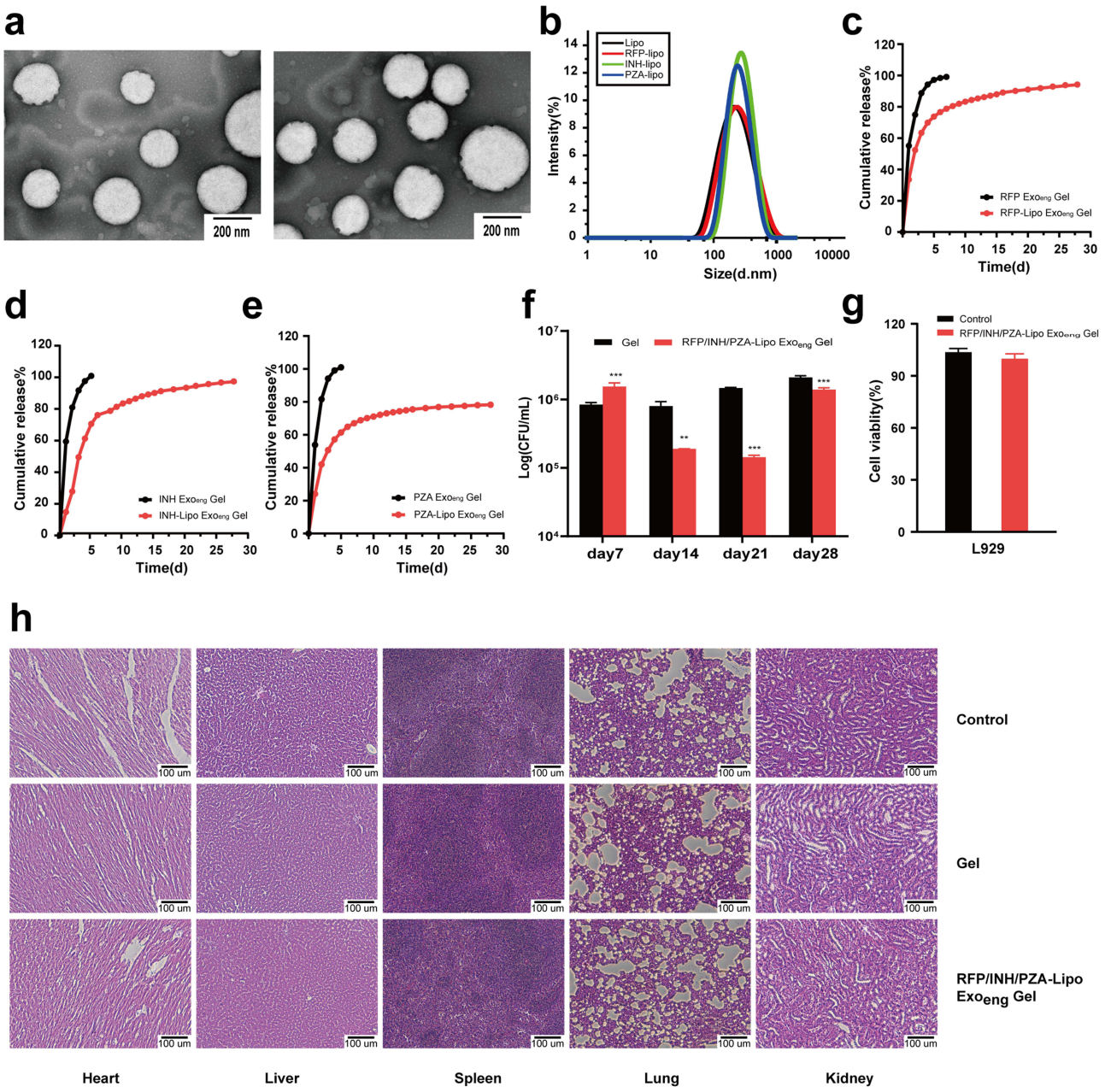

Figure 5 (**a**) TEM images of empty liposomes (left) and RFP-loaded liposomes (right). (**b**) DLS analysis of four types liposomes. (**c-e**) Release of RFP, RFP-Lipo, INH, INH-Lipo, PZA, and PZA-Lipo from Exo_{eng} Gel network. (**f**) Quantification of bacteria colonies in different degradation liquids. (**p<0.01, ***p<0.001 vs Gel group). (**g**) Effect of RFP/INH/PZA-Lipo Exo_{eng} Gel extracts on cell viability measured by CCK8 assay. (**h**) HE staining analysis of main organs in rat after implantation of RFP/INH/PZA-Lipo Exo_{eng} Gel for 4 weeks (Exo_{eng}: Fe_3O_4-AMF-Exo).

we utilize liposomes to achieve sustained release of triple anti-tuberculosis drugs, minimizing potential physical interactions between the drugs at the same time. Moreover, multi-drug combination therapy is necessary for treating TB and other infectious diseases, it also provides new ideas for the treatment of various diseases. There are also some shortcomings in this study. The composition ratio of liposomes was not optimized in this manuscript, we just chose a ratio according reference and got the intact liposomes. It is not enough for further clinical application. More details should be explored, such as the proportion of liposomes with the best encapsulation efficiency, and whether liposomes with different proportions affect the drug release. These thoughts could help the designed scaffold close to clinical translation.

https://doi.org/10.2147/IJN.S480288

Table 1 MIC of Each Group Against H37Rv

Group	MIC (μg/mL)
RFP	0.25
RFP-Lipo Exo_{eng} Gel	0.25
INH	0.0625
INH-Lipo Exo_{eng} Gel	0.0625
PZA	300
PZA-Lipo Exo_{eng} Gel	300

Abbreviations: BJTB, bone and joint tuberculosis; Exo_{eng}, engineered exosomes; TB, Tuberculosis; EPTB, extrapulmonary tuberculosis; RFP, rifampicin; MSCs, mesenchymal stem cells; BMSCs, bone mesenchymal stem cells; OHA, oxidized hyaluronic acid; CMCS, carboxymethyl chitosan; INH, isoniazid; PZA, pyrazinamide; HAP, hydroxyapatite; AMF, alternating magnetic fields; HUVECs, Human Umbilical Vein Endothelial Cells; ALP, Alkaline Phosphatase; ARS, Alizarin Red Staining; RUNX2, Runt-associated transcription factor 2; OPN, Osteopontin; COL1A1, Collagen type I alpha 1; MIC, minimum inhibitory concentration.

Antibacterial Activity of RFP/INH/PZA-Lipo Exo_{eng} Gel

The antimicrobial activity against M. tuberculosis (H37Rv) of the drug-loaded liposomes compared to that of the drug alone was determined using minimum inhibitory concentration[28] assays. As indicated in Table 1, the MICs of RFP and RFP-Lipo Gel were 0.25 μg/mL against H37Rv, while that of both INH and INH-Lipo Gel were 0.0625 μg/mL. Additionally, PZA and PZA-Lipo Gel exhibited MICs of 300 μg/mL against H37Rv. These data indicate that encapsulating RFP, INH, or PZA in liposomes does not affect their antimicrobial activity. In coated plate experiments, we used degradation fluid taken on days 7, 14, 21, and 28 from both scaffolds to verify the release and effectiveness of the antituberculosis drug. As shown in Figure 5f, from day 14 onward, the RFP/INH/PZA-Lipo Exo_{eng} Gel degradation fluid exhibited stronger inhibition than did the Gel group degradation fluid. This confirms that the RFP/INH/PZA-Lipo Exo_{eng} Gel contains effective anti-tuberculosis drugs, and its antimicrobial effect lasts for at least 28 days. As drug vehicles, liposomes exhibit outstanding properties, such as extending the half-life of the drug, controlling the release of drug molecules, and excellent biocompatibility and safety.[77,78] In clinical applications, liposomal drugs have been proven to be most useful for their ability to reduce the side effects of the encapsulated drugs relative to free drugs.[79] To extend duration of drug release, liposomes were designed to load drugs and added to the Gel. The RFP/INH/PZA-Lipo Exo_{eng} Gel shows a well antimicrobial activity against *Mycobacterium tuberculosis*.

Biosafety of RFP/INH/PZA-Lipo Exo_{eng} Gel

The biocompatibility of materials, both in vivo and in vitro, is a critical factor in assessing the suitability of injectable hydrogels for clinical use as biomedical materials. We used the leachate method[80] to examine the impact of the RFP/INH/PZA-Lipo Exo_{eng} Gel extract on L929 cells. As shown in Figure 5g, the cells exhibited a relative proliferation rate of over 90% with no cytotoxicity. Subsequently, we evaluated the in vivo safety of RFP/INH/PZA-Lipo Exo_{eng} Gel. After a rat femoral ankle defect model was generated, the scaffold was implanted into the defect. Blood samples were collected from the rats at 1, 2, and 4 weeks after surgery, and their organs were removed postmortem. The serum levels of AST and Cr were measured, and these results are presented in Table S2. All the values for each group were within the normal reference range. Paraffin sectioning and hematoxylin and eosin (HE) staining were conducted on the hearts, livers, spleens, lungs, and kidneys of the rats. Microscopy revealed no apparent tissue damage in the organs of each group, suggesting that the scaffolds exhibited high biosafety (Figure 5h). The above results indicate that the RFP/INH/PZA-Lipo

Exo_{eng} Gel has good biosafety, which shown the scaffold is a potential candidate for studying the therapeutic effect of bone tuberculosis animal models.

Conclusion

This study developed a biomimetic artificial bone composite scaffold drug delivery system for the treatment of bone and joint tuberculosis. The system demonstrated bioactivities such as injectability, self-healing, exosome release, and antibacterial activity, promoted angiogenesis and osteogenesis and sustained RFP/INH/PZA release for 28 days. However, within the intricate in vivo environment, further research is required to determine if the drug can be consistently and stably released over a period exceeding 28 days to achieve the long-term therapeutic goals of BJTB effectively. We will follow up to verify inhibition of H37Rv infection in vivo that slowly releases anti-tuberculosis drugs and assess the effectiveness of bone defect repair using the RFP/INH/PZA-Lipo Exo_{eng} Gel system. The composite scaffold was highly compatible with biological tissues, making it a promising candidate for animal models. The drug-loaded hydrogel on implantable devices are believe to be a universal method not only for the advanced treatment of BJTB, but for other local infection.

Ethics Approval and Consent to Participate

All animal procedures were performed according to the Institutional Animal Care & Use Committee at the The Second Hospital of Nanjing. Ethics approval number: 2018-LS-ky017. The animal studies were approved by the Experimental Animal Ethics Committee of Nanjing University of Chinese Medicine. All animals received humane care in compliance with the Principles of Laboratory Animal Care formulated by the National Society for Medical Research.

Author Contributions

All authors made a significant contribution to the work reported, whether that is in the conception, study design, execution, acquisition of data, analysis and interpretation, or in all these areas; took part in drafting, revising or critically reviewing the article; gave final approval of the version to be published; have agreed on the journal to which the article has been submitted; and agree to be accountable for all aspects of the work.

Funding

This work was supported by the Social Development Project of the Key Research and Development Plan of Jiangsu Province (BE2023660), the Innovation Center for Infectious Diseases of Jiangsu Province (CXZX202232),"333 Talent Project" of Jiangsu province, the Graduate Innovation Plan Project of Jiangsu Province (SJCX23_0854, KYCX24_2179), and China Postdoctoral Science Foundation (Certificate Number: 2023M743559).

Disclosure

The authors have declared that no competing interest exists.

References

1. WHO. Global Tuberculosis reports. Available from: https://www.who.int/teams/global-tuberculosis-programme/tb-reports. Accessed January 04, 2025.
2. Sharma SK, Mohan A, Kohli M. Extrapulmonary tuberculosis. *Expert Rev Respir Med*. 2021;15(7):931–948. doi:10.1080/17476348.2021.1927718
3. Kay AW, Ness T, Verkuijl SE, et al. Xpert MTB/RIF Ultra assay for tuberculosis disease and rifampicin resistance in children. *Cochrane Database Syst Rev*. 2022;9(9):CD013359. doi:10.1002/14651858.CD013359.pub3
4. Ge Z, Wang Z, Wei M. Measurement of the concentration of three antituberculosis drugs in the focus of spinal tuberculosis. *Eur Spine J*. 2008;17 (11):1482–1487. doi:10.1007/s00586-008-0778-7
5. Yang S, Zhu B, Yin P, et al. Integration of human umbilical cord mesenchymal stem cells-derived exosomes with hydroxyapatite-embedded hyaluronic acid-alginate hydrogel for bone regeneration. *ACS Biomater Sci Eng*. 2020;6(3):1590–1602. doi:10.1021/acsbiomaterials.9b01363
6. Li Y, Li L, Sha X, et al. Instant hydrogelation encapsulates drugs onto implants intraoperatively against osteoarticular tuberculosis. *J Mater Chem B*. 2021;9(38):8056–8066. doi:10.1039/d1tb00997d
7. Aoki K, Saito N. Biodegradable polymers as drug delivery systems for bone regeneration. *Pharmaceutics*. 2020;12(2):95. doi:10.3390/pharmaceutics12020095

8. Li L, Wang N, Jin X, et al. Biodegradable and injectable in situ cross-linking chitosan-hyaluronic acid based hydrogels for postoperative adhesion prevention. *Biomaterials*. 2014;35(12):3903–3917. doi:10.1016/j.biomaterials.2014.01.050
9. Yan S, Ren J, Jian Y, Wang W, Yun W, Yin J. Injectable maltodextrin-based micelle/hydrogel composites for simvastatin-controlled release. *Biomacromolecules*. 2018;19(12):4554–4564. doi:10.1021/acs.biomac.8b01234
10. Yahia S, Khalil IA, El-Sherbiny IM. Dual antituberculosis drugs-loaded gelatin hydrogel bioimplant for treating spinal tuberculosis. *Int J Pharm*. 2023;633:122609. doi:10.1016/j.ijpharm.2023.122609
11. Doyle LM, Wang MZ. Overview of extracellular vesicles, their origin, composition, purpose, and methods for exosome isolation and analysis. *Cells*. 2019;8(7):727. doi:10.3390/cells8070727
12. Song X, Xu L, Zhang W. Biomimetic synthesis and optimization of extracellular vesicles for bone regeneration. *J Control Release*. 2023;355:18–41. doi:10.1016/j.jconrel.2023.01.057
13. Zou Y, Li L, Li Y, et al. Restoring cardiac functions after myocardial infarction-ischemia/reperfusion via an exosome anchoring conductive hydrogel. *ACS Appl Mater Interfaces*. 2021;13(48):56892–56908. doi:10.1021/acsami.1c16481
14. Chen A, Tian H, Yang N, et al. Towards extracellular vesicle delivery systems for tissue regeneration: material design at the molecular level. *Extracellular Vesicles Circulating Nucleic Acids*. 2022;3(4):306–339. doi:10.20517/evcna.2022.37
15. Wang C, Wang M, Xu T, et al. Engineering bioactive self-healing antibacterial exosomes hydrogel for promoting chronic diabetic wound healing and complete skin regeneration. *Theranostics*. 2019;9(1):65–76. doi:10.7150/thno.29766
16. Bei HP, Hung PM, Yeung HL, Wang S, Zhao X. Bone-a-petite: engineering exosomes towards bone, osteochondral, and cartilage repair. *Small*. 2021;17(50). doi:10.1002/smll.202101741
17. Liu H, Geng Z, Su J. Engineered mammalian and bacterial extracellular vesicles as promising nanocarriers for targeted therapy. *Extracellular Vesicles Circulating Nucleic Acids*. 2022;3(1):63–86. doi:10.20517/evcna.2022.04
18. Wu D, Chang X, Tian J, et al. Bone mesenchymal stem cells stimulation by magnetic nanoparticles and a static magnetic field: release of exosomal miR-1260a improves osteogenesis and angiogenesis. *J Nanobiotechnology*. 2021;19(1):209. doi:10.1186/s12951-021-00958-6
19. Liu X, Wu C, Zhang Y, et al. Hyaluronan-based hydrogel integrating exosomes for traumatic brain injury repair by promoting angiogenesis and neurogenesis. *Carbohydr Polym*. 2023;306:120578. doi:10.1016/j.carbpol.2023.120578
20. Abdelaziz D, Hefnawy A, Al-Wakeel E, El-Fallal A, El-Sherbiny IM. New biodegradable nanoparticles-in-nanofibers based membranes for guided periodontal tissue and bone regeneration with enhanced antibacterial activity. *J Adv Res*. 2021;28:51–62. doi:10.1016/j.jare.2020.06.014
21. Yuan L, Wu Y, Gu QS, El-Hamshary H, El-Newehy M, Mo X. Injectable photo crosslinked enhanced double-network hydrogels from modified sodium alginate and gelatin. *Int J Biol Macromol*. 2017;96:569–577. doi:10.1016/j.ijbiomac.2016.12.058
22. Wang X, Xu D, Lv W, et al. Synthesis and drug release of Fe_3O_4@ZIF-8@PA, an anticancer drug-carrying system. *J Chem High Educ*. 2017;38 (11):1927–1934.
23. Zhou J, Ming LG, Ge BF, et al. Effects of 50 hz sinusoidal electromagnetic fields of different intensities on proliferation, differentiation and mineralization potentials of rat osteoblasts. *Bone*. 2011;49(4):753–761. doi:10.1016/j.bone.2011.06.026
24. Jia G, Han Y, An Y, et al. NRP-1 targeted and cargo-loaded exosomes facilitate simultaneous imaging and therapy of glioma in vitro and in vivo. *Biomaterials*. 2018;178:302–316. doi:10.1016/j.biomaterials.2018.06.029
25. Chen Z, Wang L, Guo C, et al. Vascularized polypeptide hydrogel modulates macrophage polarization for wound healing. *Acta Biomater*. 2023;155:218–234. doi:10.1016/j.actbio.2022.11.002
26. Srihera N, Li Y, Zhang TT, et al. Preparation and characterization of astaxanthin-loaded liposomes stabilized by sea cucumber sulfated sterols instead of cholesterol. *J Oleo Sci*. 2022;71(3):401–410. doi:10.5650/jos.ess21233
27. Chen Y, He N, Yang T, et al. Fucoxanthin loaded in palm stearin- and cholesterol-based solid lipid nanoparticle-microcapsules, with improved stability and bioavailability in vivo. *Mar Drugs*. 2022;20(4):237. doi:10.3390/md20040237
28. Familtseva A, Jeremic N, Tyagi SC. Exosomes: cell-created drug delivery systems. *Mol Cell Biochem*. 2019;459(1–2):1–6. doi:10.1007/s11010-019-03545-4
29. Hofreiter BT, Alexander BH, Wolff IA. Rapid estimation of dialdehyde content of periodate oxystarch through quantitative alkali consumption. *Anal Chem*. 1955;27(12):1930–1931. doi:10.1021/ac60108a023
30. Li S, Pei M, Wan T, et al. Self-healing hyaluronic acid hydrogels based on dynamic Schiff base linkages as biomaterials. *Carbohydr Polym*. 2020;250:116922. doi:10.1016/j.carbpol.2020.116922
31. Park H, Choi B, Hu J, Lee M. Injectable chitosan hyaluronic acid hydrogels for cartilage tissue engineering. *Acta Biomater*. 2013;9(1):4779–4786. doi:10.1016/j.actbio.2012.08.033
32. Ding Z, Han H, Fan Z, et al. Nanoscale silk-hydroxyapatite hydrogels for injectable bone biomaterials. *ACS Appl Mater Interfaces*. 2017;9 (20):16913–16921. doi:10.1021/acsami.7b03932
33. Radasch RM. Biomechanics of bone and fractures. *Vet Clin North Am Small Anim Pract*. 1999;29(5):1045–82,v–vi. doi:10.1016/s0195-5616(99) 50102-2
34. Lee SS, Kim JH, Jeong J, et al. Sequential growth factor releasing double cryogel system for enhanced bone regeneration. *Biomaterials*. 2020;257:120223. doi:10.1016/j.biomaterials.2020.120223
35. Xu Y, Xu C, He L, et al. Stratified-structural hydrogel incorporated with magnesium-ion-modified black phosphorus nanosheets for promoting neuro-vascularized bone regeneration. *Bioact Mater*. 2022;16:271–284. doi:10.1016/j.bioactmat.2022.02.024
36. Zou W, Zhao J, Li Y, et al. Rat bone marrow-derived mesenchymal stem cells promote the migration and invasion of colorectal cancer stem cells. *Onco Targets Ther*. 2020;13:6617–6628. doi:10.2147/ott.S249353
37. Racchetti G, Meldolesi J. Four distinct cytoplasmic structures generate and release specific vesicles, thus opening the way to intercellular communication. *Extracellular Vesicles Circulating Nucleic Acids*. 2023;4(1):44–58. doi:10.20517/evcna.2023.03
38. Lin J, Wang Z, Huang J, et al. Microenvironment-protected exosome-hydrogel for facilitating endometrial regeneration, fertility restoration, and live birth of offspring. *Small*. 2021;17(11):e2007235. doi:10.1002/smll.202007235
39. Li H, Ding Y, Huang J, et al. Angiopep-2 modified exosomes load rifampicin with potential for treating central nervous system tuberculosis. *Int J Nanomed*. 2023;18:489–503. doi:10.2147/IJN.S395246
40. Li W, Liu Y, Zhang P, et al. Tissue-engineered bone immobilized with human adipose stem cells-derived exosomes promotes bone regeneration. *ACS Appl Mater Interfaces*. 2018;10(6):5240–5254. doi:10.1021/acsami.7b17620

41. Wang Y, Zhang S, Benoit DSW. Degradable poly(ethylene glycol) (PEG)-based hydrogels for spatiotemporal control of siRNA/nanoparticle delivery. *J Control Release*. 2018;287:58–66. doi:10.1016/j.jconrel.2018.08.002
42. Han Y, Jiang L, Shi H, et al. Effectiveness of an ocular adhesive polyhedral oligomeric silsesquioxane hybrid thermo-responsive FK506 hydrogel in a murine model of dry eye. *Bioact Mater*. 2022;9:77–91. doi:10.1016/j.bioactmat.2021.07.027
43. Tottoli EM, Dorati R, Genta I, Chiesa E, Pisani S, Conti B. Skin wound healing process and new emerging technologies for skin wound care and regeneration. *Pharmaceutics*. 2020;12(8):735. doi:10.3390/pharmaceutics12080735
44. Rehman SRU, Augustine R, Zahid AA, Ahmed R, Tariq M, Hasan A. Reduced graphene oxide incorporated GelMA hydrogel promotes angiogenesis for wound healing applications. *Int J Nanomed*. 2019;14:9603–9617. doi:10.2147/ijn.S218120
45. Ruan S, Rody WJ, Patel SS, et al. Receptor activator of nuclear factor-kappa B is enriched in CD9-positive extracellular vesicles released by osteoclasts. *Extracell Vesicles Circ Nucl Acids*. 2023;4(3):518–529. doi:10.20517/evcna.2023.38
46. Zhou Y, Zhang XL, Lu ST, et al. Human adipose-derived mesenchymal stem cells-derived exosomes encapsulated in pluronic F127 hydrogel promote wound healing and regeneration. *Stem Cell Res Ther*. 2022;13(1):407. doi:10.1186/s13287-022-02980-3
47. Lu L, Shen L, Cui S, et al. Angiogenic activity and mechanism for bisphenols on endothelial cell and mouse: evidence of a structural-selective effect. *Environ Sci Technol*. 2023;57(32):11803–11813. doi:10.1021/acs.est.3c03883
48. Lee SG, Kim JS, Kim HJ, Schlaepfer DD, Kim IS, Nam JO. Endothelial angiogenic activity and adipose angiogenesis is controlled by extracellular matrix protein TGFBI. *Sci Rep*. 2021;11(1):9644. doi:10.1038/s41598-021-88959-1
49. Wang D, Cao H, Hua W, et al. Mesenchymal stem cell-derived extracellular vesicles for bone defect repair. *Membranes*. 2022;12(7). doi:10.3390/membranes12070716
50. Shi H, Zhou K, Wang M, et al. Integrating physicomechanical and biological strategies for BTE: biomaterials-induced osteogenic differentiation of MSCs. *Theranostics*. 2023;13(10):3245–3275. doi:10.7150/thno.84759
51. Halverson PB. Arthropathies associated with basic calcium phosphate crystals. *Scanning Microsc*. 1992;6(3):791–796. discussion 796-7.
52. Rong M, Liu D, Xu X, et al. A superparamagnetic composite hydrogel scaffold as in vivo dynamic monitorable theranostic platform for osteoarthritis regeneration. *Adv Mater*. 2024;36(35):e2405641. doi:10.1002/adma.202405641
53. Deng C, Li Z, Lu L, et al. Sophisticated magneto-mechanical actuation promotes in situ stem cell assembly and chondrogenesis for treating osteoarthritis. *ACS Nano*. 2023;17(21):21690–21707. doi:10.1021/acsnano.3c06909
54. Guan P, Liu C, Xie D, et al. Exosome-loaded extracellular matrix-mimic hydrogel with anti-inflammatory property Facilitates/promotes growth plate injury repair. *Bioact Mater*. 2022;10:145–158. doi:10.1016/j.bioactmat.2021.09.010
55. Kang Y, Xu C, Meng L, Dong X, Qi M, Jiang D. Exosome-functionalized magnesium-organic framework-based scaffolds with osteogenic, angiogenic and anti-inflammatory properties for accelerated bone regeneration. *Bioact Mater*. 2022;18:26–41. doi:10.1016/j.bioactmat.2022.02.012
56. Smyth T, Kullberg M, Malik N, Smith-Jones P, Graner MW, Anchordoquy TJ. Biodistribution and delivery efficiency of unmodified tumor-derived exosomes. *J Control Release*. 2015;199:145–155. doi:10.1016/j.jconrel.2014.12.013
57. García-Manrique P, Matos M, Gutiérrez G, Pazos C, Blanco-López MC. Therapeutic biomaterials based on extracellular vesicles: classification of bio-engineering and mimetic preparation routes. *J Extracell Vesicles*. 2018;7(1):1422676. doi:10.1080/20013078.2017.1422676
58. Liao Q, Li BJ, Li Y, et al. Low-intensity pulsed ultrasound promotes osteoarthritic cartilage regeneration by BMSC-derived exosomes via modulating the NF-κB signaling pathway. *Int Immunopharmacol*. 2021;97:107824. doi:10.1016/j.intimp.2021.107824
59. Liu W, Li L, Rong Y, et al. Hypoxic mesenchymal stem cell-derived exosomes promote bone fracture healing by the transfer of miR-126. *Acta Biomater*. 2020;103:196–212. doi:10.1016/j.actbio.2019.12.020
60. Meng J, Xiao B, Zhang Y, et al. Super-paramagnetic responsive nanofibrous scaffolds under static magnetic field enhance osteogenesis for bone repair in vivo. *Sci Rep*. 2013;3(1):2655. doi:10.1038/srep02655
61. Kolosnjaj-Tabi J, Javed Y, Lartigue L, et al. The one year fate of iron oxide coated gold nanoparticles in mice. *ACS Nano*. 2015;9(8):7925–7939. doi:10.1021/acsnano.5b00042
62. Zhao H, Liu C, Liu Y, et al. Harnessing electromagnetic fields to assist bone tissue engineering. *Stem Cell Res Ther*. 2023;14(1):7. doi:10.1186/s13287-022-03217-z
63. Hao Z, Ren L, Zhang Z, et al. A multifunctional neuromodulation platform utilizing Schwann cell-derived exosomes orchestrates bone microenvironment via immunomodulation, angiogenesis and osteogenesis. *Bioact Mater*. 2023;23:206–222. doi:10.1016/j.bioactmat.2022.10.018
64. Han S, Yang H, Ni X, et al. Programmed release of vascular endothelial growth factor and exosome from injectable chitosan nanofibrous microsphere-based PLGA-PEG-PLGA hydrogel for enhanced bone regeneration. *Int J Biol Macromol*. 2023;253(Pt 1):126721. doi:10.1016/j.ijbiomac.2023.126721
65. Zhang S, Chu WC, Lai RC, Lim SK, Hui JH, Toh WS. Exosomes derived from human embryonic mesenchymal stem cells promote osteochondral regeneration. *Osteoarthritis Cartilage*. 2016;24(12):2135–2140. doi:10.1016/j.joca.2016.06.022
66. Hao ZC, Lu J, Wang SZ, Wu H, Zhang YT, Xu SG. Stem cell-derived exosomes: a promising strategy for fracture healing. *Cell Prolif*. 2017;50(5). doi:10.1111/cpr.12359
67. Li B, Chen X, Qiu W, et al. Synchronous disintegration of ferroptosis defense axis via engineered exosome-conjugated magnetic nanoparticles for glioblastoma therapy. *Adv Sci*. 2022;9(17):e2105451. doi:10.1002/advs.202105451
68. Zhang M, Hu S, Liu L, et al. Engineered exosomes from different sources for cancer-targeted therapy. *Signal Transduct Target Ther*. 2023;8(1):124. doi:10.1038/s41392-023-01382-y
69. Cipolla D, Wu H, Eastman S, Redelmeier T, Gonda I, Chan HK. Tuning ciprofloxacin release profiles from liposomally encapsulated nanocrystalline drug. *Pharm Res*. 2016;33(11):2748–2762. doi:10.1007/s11095-016-2002-5
70. Halwani M, Mugabe C, Azghani AO, Lafrenie RM, Kumar A, Omri A. Bactericidal efficacy of liposomal aminoglycosides against Burkholderia cenocepacia. *J Antimicrob Chemother*. 2007;60(4):760–769. doi:10.1093/jac/dkm289
71. Natsaridis E, Gkartziou F, Mourtas S, et al. Moxifloxacin liposomes: effect of liposome preparation method on physicochemical properties and antimicrobial activity against staphylococcus epidermidis. *Pharmaceutics*. 2022;14(2):370. doi:10.3390/pharmaceutics14020370
72. Kaniga K, Cirillo DM, Hoffner S, et al. A multilaboratory, multicountry study to determine mic quality control ranges for phenotypic drug susceptibility testing of selected first-line antituberculosis drugs, second-line injectables, fluoroquinolones, clofazimine, and linezolid. *J Clin Microbiol*. 2016;54(12):2963–2968. doi:10.1128/jcm.01138-16

73. Santos NCS, Scodro RBL, de Almeida AL, et al. Combinatory activity of linezolid and levofloxacin with antituberculosis drugs in Mycobacterium tuberculosis. *Tuberculosis*. 2018;111:41–44. doi:10.1016/j.tube.2018.05.005
74. Zhang L, Li H, Kung W. Chemotherapy of tuberculosis. *China Clinician*. 2009;37(07):10–14.
75. Ioannidis P, van Soolingen D, Mokrousov I, et al. Multidrug-resistant/extensively drug-resistant tuberculosis in Greece: predominance of Mycobacterium tuberculosis genotypes endemic in the Former Soviet Union countries. *Clin Microbiol Infect*. 2017;23(12):1002–1004. doi:10.1016/j.cmi.2017.07.002
76. Li G, Liu S, Chen Y, et al. An injectable liposome-anchored teriparatide incorporated gallic acid-grafted gelatin hydrogel for osteoarthritis treatment. *Nat Commun*. 2023;14(1):3159. doi:10.1038/s41467-023-38597-0
77. Wang N, Wang T, Li T, Deng Y. Modulation of the physicochemical state of interior agents to prepare controlled release liposomes. *Colloids Surf B Biointerfaces*. 2009;69(2):232–238. doi:10.1016/j.colsurfb.2008.11.033
78. Zeng H, Qi Y, Zhang Z, Liu C, Peng W, Zhang Y. Nanomaterials toward the treatment of Alzheimer's disease: Recent advances and future trends. *Chinese Chemical Letters*. 2021;32(6):1857–1868. doi:10.1016/j.cclet.2021.01.014
79. Allen TM, Cullis PR. Liposomal drug delivery systems: from concept to clinical applications. *Adv Drug Deliv Rev*. 2013;65(1):36–48. doi:10.1016/j.addr.2012.09.037
80. Desai DT, Maulvi FA, Desai AR, et al. In vitro and in vivo evaluation of cyclosporine-graphene oxide laden hydrogel contact lenses. *Int J Pharm*. 2022;613:121414. doi:10.1016/j.ijpharm.2021.121414

International Journal of Nanomedicine

Dovepress
Taylor & Francis Group

Publish your work in this journal

The International Journal of Nanomedicine is an international, peer-reviewed journal focusing on the application of nanotechnology in diagnostics, therapeutics, and drug delivery systems throughout the biomedical field. This journal is indexed on PubMed Central, MedLine, CAS, SciSearch®, Current Contents®/Clinical Medicine, Journal Citation Reports/Science Edition, EMBase, Scopus and the Elsevier Bibliographic databases. The manuscript management system is completely online and includes a very quick and fair peer-review system, which is all easy to use. Visit http://www.dovepress.com/testimonials.php to read real quotes from published authors.

Submit your manuscript here: https://www.dovepress.com/international-journal-of-nanomedicine-journal